PROBE MICROSCOPY

Probing and imaging spin interactions with a magnetic single-molecule sensor

Gregory Czap¹, Peter J. Wagner¹, Feng Xue², Lei Gu¹, Jie Li¹.², Jiang Yao¹, Ruqian Wu¹.²*, W. Ho¹.³*

Magnetic single atoms and molecules are receiving intensifying research focus because of their potential as the smallest possible memory, spintronic, and qubit elements. Scanning probe microscopes used to study these systems have benefited greatly from new techniques that use molecule-functionalized tips to enhance spatial and spectroscopic resolutions and enable new sensing capabilities. We demonstrate a microscopy technique that uses a magnetic molecule, Ni(cyclopentadienyl)₂, adsorbed at the apex of a scanning probe tip, to sense exchange interactions with another molecule adsorbed on a Ag(110) surface in a continuously tunable fashion in all three spatial directions. We further used the probe to image contours of exchange interaction strength, revealing angstrom-scale regions where the quantum states of two magnetic molecules strongly mix. Our results pave the way for new nanoscale imaging capabilities based on magnetic single-molecule sensors.

agnetic single atoms and molecules represent the ultimate spatial limit in magnetic memory storage, spintronics, and fundamental studies of spin-spin interactions (1). Because of recent breakthroughs in increasing the excited-spin state lifetimes (2, 3), magnetic remanence temperatures (4), and spin coherence lifetimes (5-7), these systems are now also being reconsidered as platforms for quantum computation (8, 9). There is a pressing need to develop techniques that can follow spin systems interacting with their local environment. Scanning probe microscopy (SPM) techniques offer particular experimental advantages given their ability to image single atoms and molecules as well as characterize their adsorption environments. In addition, SPM can be used to study the spin-flip dynamics by using inelastic electron tunneling spectroscopy (10, 11), probe spin density of states via spin-polarized scanning tunneling microscopy (12), sense magnetic exchange forces with atomic force microscopy (13), measure excited-spin state lifetimes in pump-probe schemes (14), and resolve electron paramagnetic resonance of single atoms (15, 16).

During the past decade, SPM tips functionalized by single molecules have provided unprecedented spatial resolution (17, 18). A single molecule at the tip apex behaves as a sensing device with functionality tunable through chemical design that can detect short-range intermolecular forces (19–21) or electrostatic fields (22, 23) generated by other

nano-objects. However, despite the breadth of spin properties and sensor functionality that designer magnetic molecules could in principle provide, the use of magnetic molecule tips as sensors of local magnetic fields or spin-spin interactions has remained challenging. Recently, it was shown that single molecules of nickelocene (NiCp2, where Cp is cyclopentadienyl) retained their S=1 spin triplet ground state upon adsorption onto the Cu(100) surface or the Cu tip apex (24) and could provide a realization of a molecular spin sensor.

Here we probed, characterized, and imaged spin-spin interactions between a NiCp₂ molecule attached to a scanning tunneling microscope (STM) tip and another NiCp2 molecule adsorbed on the Ag(110) surface. By performing inelastic electron tunneling spectroscopy (IETS) measurements of spin-flip excitations as a function of tipsurface distance, spin-spin coupling was revealed to occur across the vacuum gap between the molecules. We further demonstrate mapping of the strength of magnetic interactions between two molecules in the lateral plane by acquiring a series of IETS images, which reveal highly localized regions of concentrated excited-state spin density and features arising from quantum state mixing.

Experiments were performed in a home-built ultrahigh-vacuum STM with a base temperature of 600 mK and a magnetic field of up to 9 T oriented normal to the surface plane. The NiCp₂ molecules adsorbed on the Ag(110) were imaged as tall, elliptical donuts with semi-major axes oriented along the [001] lattice direction (Fig. 1, A and B). After positioning the STM tip over the center of a NiCp₂ molecule and performing IETS measurements, we observed a peak at 3.81 mV (Fig. 1C) that exhibited Zeeman splitting in the presence of an external magnetic field (Fig. 1D) with an effective magnetic moment of 1.78 μ_B (where μ_B is the Bohr magneton). The adsorbed

molecules evidently retained their gas-phase spin-triplet ground state: S=1, $m_{\rm s}=0$, with the IETS peaks corresponding to the $m_{\rm s}=0 \to m_{\rm s}=\pm 1$ spin-flip excitations (24). The 3.81-meV zero-field splitting was caused by the intrinsic magnetic anisotropy within the molecule, with the spin hard axis aligned with the molecular (Z) axis (25). An energy-level diagram for the single NiCp₂ system is shown in Fig. 1E.

A single NiCp2 molecule was transferred from the surface to the STM tip by bringing the tip to close approach with the surface (26). Similar spectroscopic measurements obtained with the resulting NiCp₂-tip positioned above the Ag(110) surface yielded a slightly higher magnetic anisotropy energy of 3.97 meV and effective magnetic moment of 1.89 μ_B , with some variation among tip terminations (fig. S3) (26). When the NiCp2-tip was then positioned above another NiCp2 adsorbed on the surface (Fig. 1, F and G), IETS measurements revealed splitting of the 3.81-mV spin-flip peak at zero field that arose from spin-spin interactions E_{int} , as well as a new peak at 7.35 mV (Fig. 1, H and I). In an external magnetic field $B_{\rm ext}$, the two lower-energy peaks individually split through the Zeeman effect, indicating that they both correspond to $m_s = 0 \rightarrow$ $m_{\rm s}=\pm\,1\,$ single spin-flip (SSF) excitations. By contrast, the 7.35-mV peak remained nearly unaffected by the magnetic field and was assigned to an antiferromagnetic double spin-flip (DSF) excitation in which the spins of each molecule are flipped in opposite directions ($\Delta m_s = 0$ overall), as suggested previously by Ormaza et al. (24). An energy-level diagram depicting the evolution of SSF and DSF states under the influence of $E_{\rm int}$ and B_{ext} is shown in Fig. 1J.

A series of STM-IETS spectra were then acquired at different tip heights (Fig. 2, A and B) at low magnetic field (B=1 T) (27) to study the effect of varying spin-spin interaction strength. As the intermolecular distance decreased, the initially degenerate SSF peaks split and the DSF peak redshifted. At intermediate distance, the splitting of the SSF peak was asymmetric, with the lower-energy peak redshifting less and the higher-energy peak blueshifting more, and at the smallest distances the DSF peak also split.

The coupled NiCp₂-tip/NiCp₂-surf spin system can be described by a model Hamiltonian:

$$\begin{split} \hat{H}_s &= g \mu_B B_{\text{ext}} (\hat{S}_{1z} + \hat{S}_{2z}) + D_1 (\hat{S}_{1z}^2) \\ &+ D_2 (\hat{S}_{2z}^2) + E_{\text{int}} (\vec{S}_1 \cdot \vec{S}_2) \end{split} \tag{1}$$

The first term is the Zeeman energy $E_z = g\mu_B B_{\rm ext}$ of each spin in an external magnetic field; the next two terms are the uniaxial magnetic anisotropy energies $D_{\rm i}$ of the two molecules, and the final term results from contributions of exchange $(E_{\rm ex})$ and dipole-dipole $(E_{\rm dd})$ interactions. In the present experiment, the intermolecular separation was only a few angstroms, and we found that exchange interactions were the dominant contribution to $E_{\rm int}$ (i.e., $E_{\rm int} \approx E_{\rm ex}$) (figs. S4 and S5) (26). This result is consistent with previous

¹Department of Physics and Astronomy, University of California, Irvine, CA 92697-4575, USA. ²State Key Laboratory of Surface Physics and Key Laboratory for Computational Physical Sciences (MOE) and Department of Physics, Fudan University, Shanghai, 200433, China. ³Department of Chemistry, University of California, Irvine, CA 92697-2025, USA.

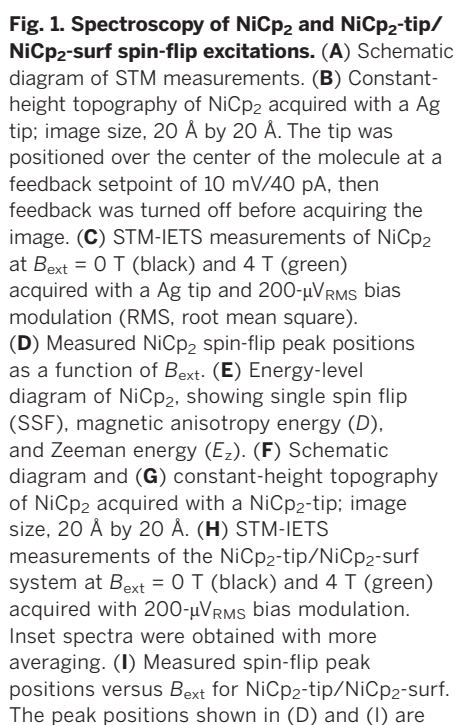
^{*}Corresponding author. Email: wilsonho@uci.edu (W.H.); wur@uci.edu (R.W.)

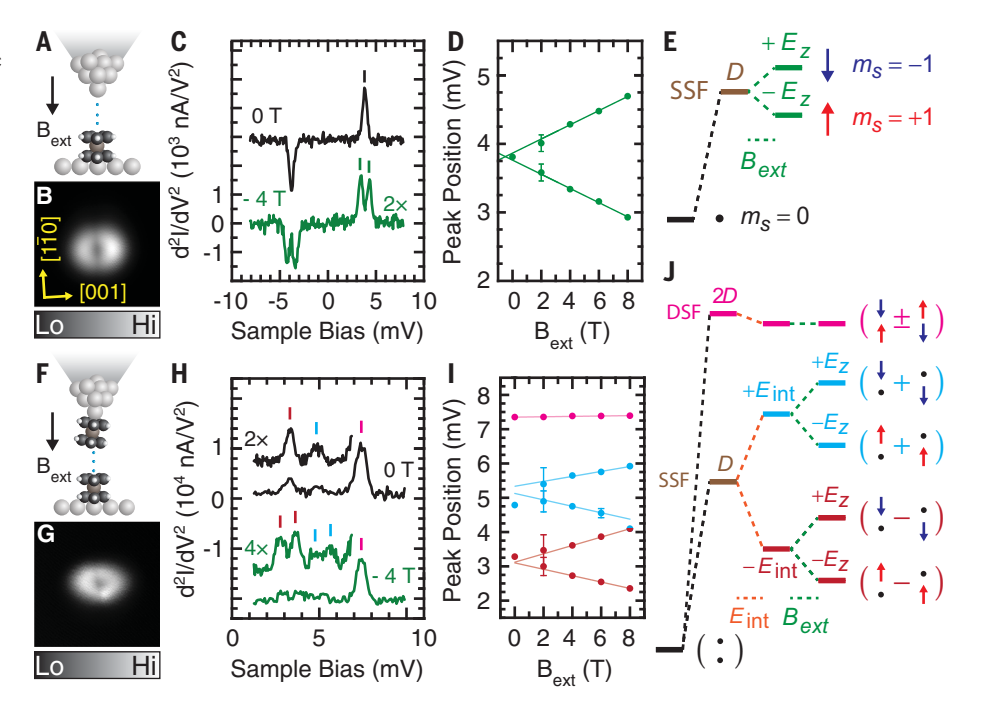
studies of spin-spin interactions between adsorbed

magnetic metal adatoms at small interatomic distances (<1 nm) (28, 29) and ensemble measurements of dimers of exchange-coupled singlemolecule magnets (30-32). Notably, the redshift of the antiferromagnetic DSF state as $E_{\rm ex}$ increased demonstrated that the exchange was antiferromagnetic in nature, as seen previously in bulk measurements of diluted NiCp₂ crystals (25).

The \hat{H}_s in Eq. 1 could be expressed as a 9×9 matrix in the two-molecule spin basis $|m_{s1}, m_{s2}\rangle$, and its eigenstates could be solved through diagonalization. The ground state has the form $|0,0\rangle$ for the uncoupled case but gradually mixes with the $\frac{1}{\sqrt{2}}(|\pm 1, \mp 1\rangle + |\mp 1, \pm 1\rangle)$ state as $E_{\rm ex}$ increases. The SSF states have the form $\frac{1}{\sqrt{2}}(|\pm 1,0\rangle \pm |0,\pm 1\rangle)$. The symmetric (+) and antisymmetric (-) SSF states are degenerate for $E_{\rm ex}$ = 0 but split by Δ =

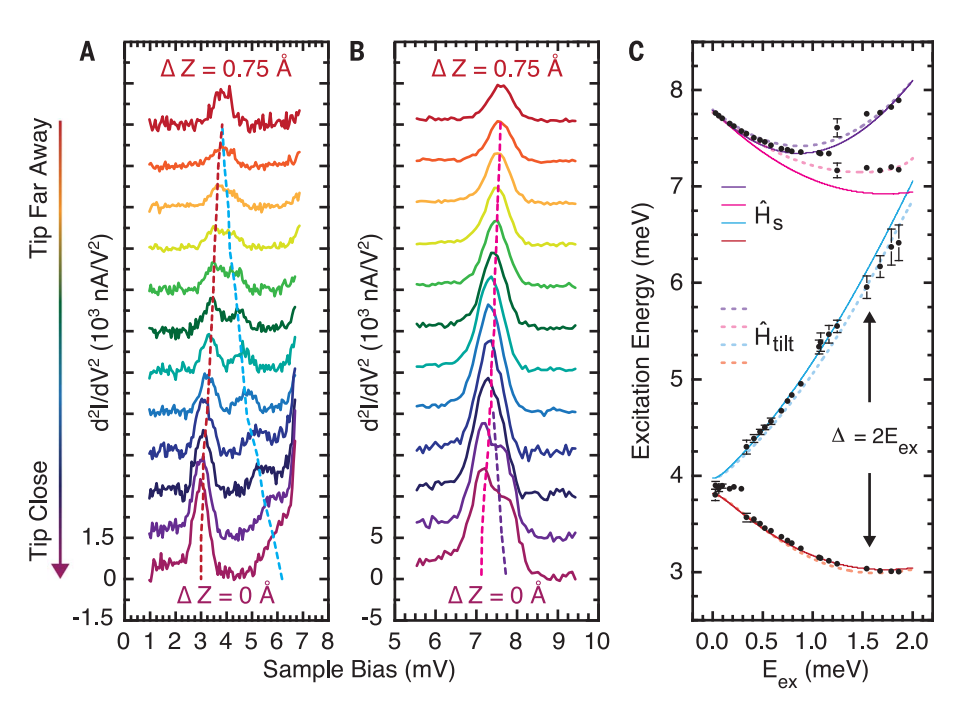
 $2E_{\rm ex}$ in the presence of exchange interactions, permitting direct assignment of $E_{\rm ex}$ from experimental measurements of the SSF peak splitting Δ . The antiferromagnetic DSF states start from $\frac{1}{\sqrt{6}}(|\pm 1, \mp 1\rangle \pm |\mp 1, \pm 1\rangle)$ and begin to mix with the $|\overset{\circ}{0},0\rangle$ ground state as E_{ex} increases. This mixing blueshifts the (+) DSF state energy but does not perturb the unmixed (-) DSF state, resulting in the observed splitting of the DSF peaks in Fig. 2B.





the average of positive and negative bias peak positions. (J) Energy-level diagram for the NiCp₂-tip/NiCp₂-surf spin system, showing SSF and DSF levels modulated by spin-spin interaction energy (E_{int}) and external magnetic field (B_{ext}).

Fig. 2. Characterization of NiCp2-tip/NiCp2-surf spin-spin interactions at varying intermolecular distances. (A) STM-IETS measurements of NiCp2-tip/NiCp2-surf SSF peaks at varying tip heights, acquired with 300-μV_{RMS} bias modulation. The tip height $\Delta Z = 1.33 \text{ Å}$ was defined by turning off the tunneling feedback loop at setpoint 70 mV/40 pA, with decreasing ΔZ corresponding to advancing the tip toward the surface in ~7-pm steps. (B) STM-IETS measurements of DSF peaks acquired at the same heights as in (A), using 200- to 300- μV_{RMS} bias modulation. (C) Comparison of measured peak positions (points) versus calculated excitation energies (curves) from the model Hamiltonian. One point is shown where peak splitting could not be resolved. Solid curves correspond to the exchange-only ($E_{dd} = 0$, $\theta_{tilt} = 0$) Hamiltonian, and dashed curves correspond to a model in which the NiCp2-tip has a tilted geometry with respect to the surface normal ($\theta_{tilt} \neq 0$) (26).



Meanwhile, the ground state energy redshifts as $E_{\rm ex}$ increases because of the gain of exchange energy.

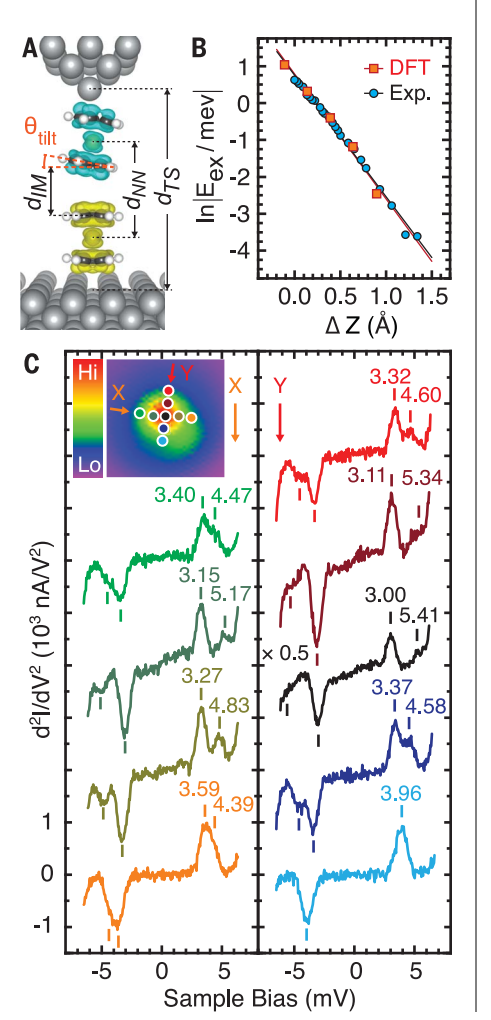
Using the eigenvalues of the ground, SSF, and DSF states of the model Hamiltonian, we found excellent agreement between the calculated excitation energies (solid curves) and the experimentally measured peak positions (black points) (Fig. 2C). No $\Delta m_s = \pm 2$ (i.e., $|0,0\rangle \rightarrow |\pm 1,\pm 1\rangle$) transitions were observed, as they are forbidden through a spin angular momentum selection rule imposed by the spin $\frac{1}{9}$ tunneling electron participating in the inelastic spin-flip excitation process. The small blueshift of the DSF excitations by 0.1 to 0.25 meV with respect to the calculated values (solid pink and purple curves) was accounted for by considering the intrinsic tilt angle of the NiCp2-tip with respect to the surface NiCp2 molecular axis [see figs. S6 to S8 and a discussion in the supplementary materials (26)].

To further our understanding of the exchange interactions, we performed density functional theory (DFT) calculations of the NiCp₂-tip/NiCp₂surf tunneling junction with the resulting relaxed geometry and spin density isosurface of the $|+1,-1\rangle$ state shown in Fig. 3A. The overall magnetic moment of each molecule was found to be distributed equally between its central Ni

Fig. 3. DFT calculations of the spin-exchange interactions and spectroscopic measurements acquired at varying lateral position.

(A) Calculated spin density isosurface $(1.5 \times 10^{-3} \text{ e} / \text{Å}^3)$ for the $|+1, -1\rangle$ state viewed from the [001] direction. The intrinsic tilt angle of the NiCp2 tip is indicated as $\theta_{\rm tilt}$, while $d_{\rm IM}$ = 4.14 Å, $d_{\rm NN}$ = 7.95 Å, and $d_{TS} = 16.65 \text{ Å refer to intermolecular}$, nickel-nickel, and tip-surface distances, respectively. (B) Comparison of E_{ex} derived from experiment and from DFT calculations. For both datasets, a best-fit of the form $y = \ln |E_0/meV| - (Z_0 + \Delta Z)/\lambda$ was used with E_0 = 2.1 meV and height offset $Z_0 = 0$ defined as in Fig. 2 for experiment and $Z_0 = 0$ defined such that $d_{TS} = 16.76$ Å for the DFT calculations. The geometry shown in (A) corresponds to the data point $\Delta Z = -0.11 \text{ Å}$ shown in (B). (C) STM-IETS measurements of NiCp2-tip/NiCp2-surf SSF peaks at varying lateral positions acquired with $500-\mu V_{RMS}$ bias modulation. The tip was positioned over the central bright spot with the feedback setpoint 70 mV/40 pA. The feedback was then turned off and the tip advanced ~1.1 Å toward the surface before repositioning the tip for both topographic and spectroscopic measurements. Inset: Constant-height STM topography of NiCp2 acquired with a NiCp₂ tip; image size, 9.7 Å by 9.7 Å.

atom and two Cp rings, indicating substantial spin polarization of the π orbitals, which overlap in the vacuum gap between the molecules. In addition, the tip-adsorbed NiCp2 was found to stabilize at a 10° angle with respect to the surface plane (θ_{tilt} in Fig. 3A), in qualitative agreement with experimental results. To characterize the spatial dependence of the spin-exchange interactions, we performed a fit of $E_{\rm ex}$ to the measured excitation energy at each height, which revealed that $E_{\rm ex}$ increased exponentially as the two molecules were brought close together (Fig. 3B, blue points). The exponential dependence of $E_{\rm ex}$ on the intermolecular separation had amplitude $E_0 \sim 2.1$ meV and decay constant $\lambda \sim 30.4$ pm, consistent with exchange interactions between magnetic metal SPM tips and magnetic adsorbates and surface layers (13, 29, 33, 34). The spinexchange interaction energy calculated at varying tip-surface separation (Fig. 3B, red squares) revealed a similar exponential decay length $\lambda \sim$ 29.6 pm, in excellent agreement with experiment. It should be noted that because the tip-surface distance is not known accurately in the experiment, it is not possible to compare the amplitude E_0 with theory. Further details and additional DFT calculations can be found in the supplementary materials (26).



The high sensitivity of $E_{\rm ex}$ to intermolecular separation motivated our study of its lateral spatial dependence. STM-IETS measurements acquired with the tip held at constant height Zand positioned at different locations in the XY plane showed changes in the magnitude of $E_{\rm ex}$ inferred from the SSF peak splitting Δ (with $E_{\rm ex}=\frac{1}{2}\Delta$). The magnitude of $E_{\rm ex}$ reached a maximum when the NiCp2-tip was directly superimposed over the surface NiCp2 and decayed rapidly as the tip was laterally repositioned away (Fig. 3C). Curiously, the interaction strength was not symmetrically distributed about the central bright spot, but decayed less rapidly above and to the left of the bright spot and more rapidly below and to the right. This asymmetry in these directions also appeared in the topography (Fig. 3C, inset) and could be plausibly explained by the twofold symmetry of the Ag(110) substrate and the tilting of the NiCp2-tip. These observations raised the tantalizing prospect of imaging contours of $E_{\rm ex}$ in real space by acquiring d^2I/dV^2 images at fixed imaging bias. A series of constantheight STM-IETS images acquired at several imaging bias values is shown in Fig. 4, A to I, along with a direct comparison to the excitation energies calculated from the model Hamiltonian (Fig. 4J). The images revealed the spatial distribution of $E_{\rm ex}$ at fixed magnitude, with the magnitude selected by the chosen imaging bias. For example, when the imaging bias was selected at 3.9 mV, spatial regions where $E_{\rm ex} \approx 0$ were imaged that corresponded to locations where the lateral intermolecular separation was large (Fig. 4F). The outer radius of signal intensity in Fig. 4, E and F, reflected a loss of tunneling current and thus spectroscopic signal rather than a shift of the SSF peak away from the imaging bias. However, regions of large $E_{\rm ex}$ were found when the $NiCp_2$ -tip was positioned directly over the surface $NiCp_2$ (Fig. 4, B to D, H, and I). In contrast to the other images, Fig. 4A did not simply visualize the spatial distribution of a single value of $E_{\rm ex}$. Instead, regions of both low $E_{\rm ex}$ (outer ring feature) and high $E_{\rm ex}$ (inner dot feature) were visualized, but intermediate values of $E_{\rm ex}$ were dim. This contrast arose from the DSF peak initially redshifting away from the 7.7-mV imaging bias at intermediate intermolecular separations and then blueshifting back when $E_{\rm ex}$ became larger than 1.0 meV as the NiCp2-tip was positioned sufficiently near to the surface NiCp₂. The ~1.5-Å-diameter spot at the center of the image corresponds to the small spatial region in which the (+) DSF state had become substantially mixed with the ground state, demonstrating the capability of this technique to spatially map and visualize quantum state mixing in real space.

The exchange-induced energy shifts and mixing of spin states demonstrated here can potentially be exploited to detect and distinguish between magnetic entities with different spin configurations. For example, calculations show that $S = \frac{1}{2}$ and $S = \frac{3}{9}$ spins could be independently imaged with a NiCp₂-tip, providing opportunities to detect and characterize unknown magnetic adsorbates and dangling bonds at surfaces [see fig. S9

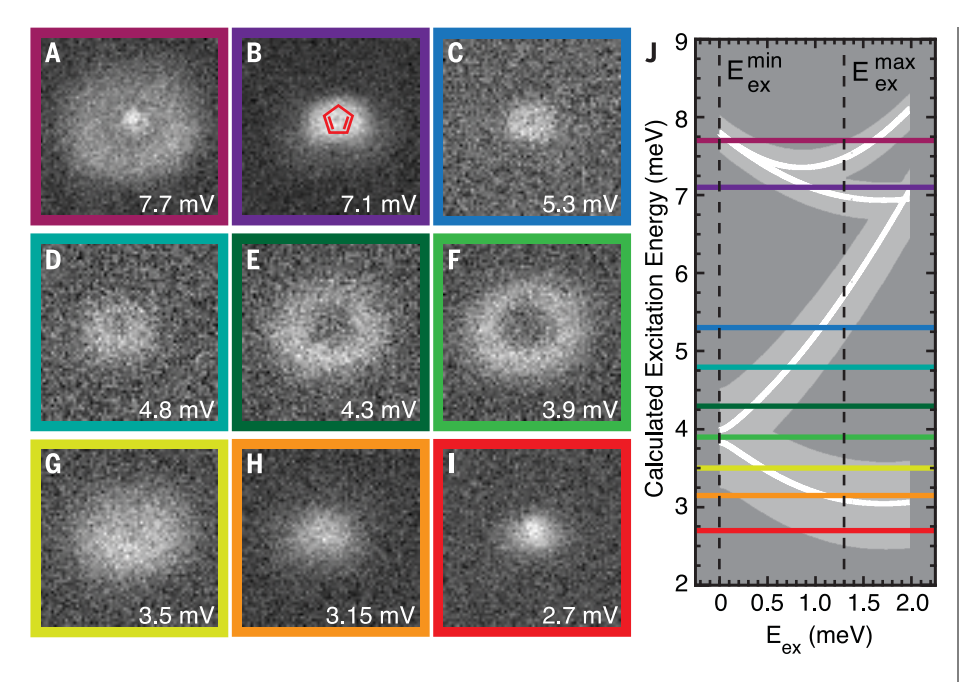


Fig. 4. Imaging contours of spin-exchange interaction strength. (A to I) Series of constant-height d²I/dV² images of a NiCp₂ molecule acquired with a NiCp₂-terminated tip at different sample biases. For each image, the tip was first positioned over the central bright spot at feedback setpoint 70 mV/40 pA, and then feedback was turned off. The tip was then advanced ~1.1 Å toward the surface before the d^2I/dV^2 image was acquired. Images (A) and (B) were acquired with 200- μV_{RMS} lock-in modulation, whereas images (C) to (I) were acquired with 500- μV_{RMS} lock-in modulation. All images are 14 Å by 14 Å, and a top view of a scaled schematic structure of NiCp2 is overlaid in (B). (J) Plot of calculated spin-flip excitation energies with each imaging bias indicated as a colored horizontal line. For simplicity θ_{tilt} is neglected. The finite widths of the single spin-flip and double spin-flip curves, depicted as thick gray outlines centered on each white curve, represent broadening due to the bias modulation. The approximate minimum and maximum values of $E_{\rm ex}$ probed in the imaging series are indicated by the vertical dashed lines.

and accompanying discussion in the supplementary materials (26)]. Ferromagnetic thin films impose an exchange bias on the NiCp2 spin states, permitting detection of surface spin densities as demonstrated recently by Verlhac et al. (35). The easily reproduced tip spin configuration and the ability to detect magnetic interactions without requiring an external magnetic field present advantages over spin-polarized STM, magnetic exchange force microscopy, and electron spin resonance-based detection schemes (12-16). In addition, the NiCp₂-tip spin states are sensitive only to magnetic interactions and are therefore free of nonmagnetic signal artifacts that must be removed in the case of the former two techniques. The use of a molecular probe tip with $m_s \neq 0$ spin ground state may enable spin-polarized tunneling current and exchangeforce microscopy measurements, potentially offering new and simpler routes to tip preparation than existing techniques.

It is also important to contrast the IETSbased detection scheme used in this study with the electron spin resonance STM techniques that can probe and image magnetic interactions between adatoms on surfaces (15, 16). Although the use of radiofrequency offers superior energy resolution compared to IETS, the practical upper frequency limit precludes probing states with excitation energies beyond a few hundred microelectron volts. In these respects, the approach demonstrated here complements and extends existing techniques while providing a platform for further experimental innovations and theoretical analyses.

The ability to measure and continuously tune spin-exchange interactions on subangstrom length scales between a magnetic molecule probe tip and magnetic adsorbates heralds the development of a new class of scanning probe sensors based on single-molecule magnets. A central advantage of this approach is that the sensor functionality can be tuned through chemical design, allowing control over spin states, excited-state lifetimes, magnetic anisotropy magnitude and direction, and spin coherence lifetimes. These capabilities could enable new directions in atomic-scale research in magnetism, spin-logic operations, and the coupling of spin qubits to their local environment. Analogous to the force-sensing capabilities of carbon monoxide-terminated tips that have become commonplace in the imaging of chemical structures on surfaces, we anticipate that spin-sensing probes based on single magnetic molecules will similarly become widely adopted.

REFERENCES AND NOTES

- L. Bogani, W. Wernsdorfer, Nat. Mater. 7, 179-186 (2008).
- F. Donati et al., Science 352, 318-321 (2016).
- F. D. Natterer et al., Nature 543, 226-228 (2017).
- C. A. P. Goodwin, F. Ortu, D. Reta, N. F. Chilton, D. P. Mills, Nature 548, 439-442 (2017).
- C.-J. Yu et al., J. Am. Chem. Soc. 138, 14678-14685 (2016).
- M. Atzori et al., J. Am. Chem. Soc. 138, 11234-11244
- K. S. Pedersen et al., J. Am. Chem. Soc. 138, 5801-5804 (2016)
- 8. Y.-S. Ding, Y.-F. Deng, Y.-Z. Zheng, Magnetochemistry 2, 40 (2016)
- L. Escalera-Moreno, J. J. Baldoví, A. Gaita-Ariño, E. Coronado, Chem. Sci. 9, 3265-3275 (2018).
- 10. B. C. Stipe, M. A. Rezaei, W. Ho, Science 280, 1732-1735
- A. J. Heinrich, J. A. Gupta, C. P. Lutz, D. M. Eigler, Science 306, 466-469 (2004).
- R. Wiesendanger, H. Güntherodt, G. Güntherodt, R. J. Gambino, R. Ruf, Phys. Rev. Lett. 65, 247-250 (1990).
- 13. U. Kaiser, A. Schwarz, R. Wiesendanger, Nature 446, 522-525
- 14. S. Loth, M. Etzkorn, C. P. Lutz, D. M. Eigler, A. J. Heinrich, Science 329, 1628-1630 (2010).
- 15. S. Baumann et al., Science 350, 417-420 (2015).
- 16. P. Willke, K. Yang, Y. Bae, A. J. Heinrich, C. P. Lutz, arXiv:1807.08944 [cond-mat.mes-hall] (24 July 2018).
- 17. L. Gross, F. Mohn, N. Moll, P. Liljeroth, G. Meyer, Science 325, 1110-1114 (2009).
- 18. C.-L. Chiang, C. Xu, Z. Han, W. Ho, Science 344, 885-888 (2014)
- 19. C. Weiss et al., Phys. Rev. Lett. 105, 086103 (2010).
- 20. P. Hapala et al., Phys. Rev. B 90, 085421 (2014).
- 21. P. Hapala, R. Temirov, F. S. Tautz, P. Jelínek, Phys. Rev. Lett. **113**, 226101 (2014).
- 22. C. Wagner et al., Phys. Rev. Lett. 115, 026101 (2015). 23. P. Hapala et al., Nat. Commun. 7, 11560 (2016).
- 24. M. Ormaza et al., Nano Lett. 17, 1877-1882 (2017).
- 25. P. Baltzer, A. Furrer, J. Hulliger, A. Stebler, Inorg. Chem. 27,
- 1543-1548 (1988).
- 26. See supplementary materials for more details.
- 27. A low magnetic field B = 1 T was used to mechanically stabilize the STM scanner via eddy current damping, ensuring higher accuracy in tip positioning. The resulting Zeeman effect can be neglected.
- 28. T. Choi et al., Nat. Nanotechnol. 12, 420-424 (2017).
- 29. K. Yang et al., Phys. Rev. Lett. 119, 227206 (2017).
- 30. S. Hill, R. S. Edwards, N. Aliaga-Alcalde, G. Christou, Science 302. 1015-1018 (2003).
- 31. R. Tiron, W. Wernsdorfer, D. Foguet-Albiol, N. Aliaga-Alcalde, G. Christou, Phys. Rev. Lett. 91, 227203 (2003).
- 32. A. Candini et al., Phys. Rev. Lett. 104, 037203 (2010).
- 33. R. Schmidt et al., Phys. Rev. Lett. 106, 257202 (2011).
- 34. S. Yan, D.-J. Choi, J. A. J. Burgess, S. Rolf-Pissarczyk, S. Loth, Nat Nanotechnol 10 40-45 (2015)
- 35. B. Verlhac et al., arXiv:1901.04862 [cond-mat.mes-hall] (27 April 2019).

ACKNOWLEDGMENTS

Funding: This work was supported by the National Science Foundation under Award no. DMR-1809127 and by the CNSF under Grant no. 11474056. Author contributions: Experiments were carried out by G.C., P.J.W., J.Y., and W.H., and calculations were performed by F.X., L.G., J.L., and R.W. Competing interests: The authors declare no competing interests. Data and materials availability: All the data are available in the main text and the supplementary

SUPPLEMENTARY MATERIALS

science.sciencemag.org/content/364/6441/670/suppl/DC1 Materials and Methods Supplementary Text Figs. S1 to S9 Table S1 References (36-41)

23 January 2019; accepted 16 April 2019 10.1126/science.aaw7505



Probing and imaging spin interactions with a magnetic single-molecule sensor

Gregory Czap, Peter J. Wagner, Feng Xue, Lei Gu, Jie Li, Jiang Yao, Rugian Wu and W. Ho

Science **364** (6441), 670-673. DOI: 10.1126/science.aaw7505

Visualizing superexchange interactions

The resolution that can be achieved in scanning probe microscopy can be greatly enhanced by absorbing a molecule such as CO on the probe tip. Czap et al. now show that this approach can be used to scan spin and magnetic properties of molecules on a surface. They adsorbed a magnetic molecule, Ni(cyclopentadienyl) 2, on a silver surface and then transferred one of these molecules to a scanning tunnel microscope tip. They could then bring the tip toward the adsorbate-covered surface and map out the strength of superexchange interactions.

Science, this issue p. 670

ARTICLE TOOLS	http://science.sciencemag.org/content/364/6441/670
SUPPLEMENTARY MATERIALS	http://science.sciencemag.org/content/suppl/2019/05/15/364.6441.670.DC1
REFERENCES	This article cites 40 articles, 8 of which you can access for free http://science.sciencemag.org/content/364/6441/670#BIBL
PERMISSIONS	http://www.sciencemag.org/help/reprints-and-permissions

Use of this article is subject to the Terms of Service